Vol. 669: 51–63, 2021
https://doi.org/10.3354/meps13722

MARINE ECOLOGY PROGRESS SERIES
Mar Ecol Prog Ser

Published July 8

Biogenic structures and cable bacteria interactions: redox domain residence times and the generation of complex pH distributions

Hang Yin, Robert C. Aller*, Qingzhi Zhu, Josephine Y. Aller

School of Marine and Atmospheric Sciences, Stony Brook University, Stony Brook, NY 11794-5000, USA

ABSTRACT: Cable bacteria are multicellular filamentous bacteria that conduct electrons nonlocally between anoxic and oxic sediment regions, creating characteristic electrogenic pH fingerprints. These microbes aggregate in 3D patterns near biogenic structures, and filament fragments are also dispersed throughout deposits. Utilizing pH-sensitive planar optodes to investigate the dynamic response of electrogenic pH fingerprints to sediment reworking, we found that mobile bioturbators like nereid polychaetes (ragworms) can disturb the pH signatures. Sudden sediment disturbance associated with burrows at sub- to multi-centimeter scales eliminates detection of pH signatures. However, electrogenic pH fingerprints can recover in as little as 13 h near abandoned, closed burrows. Sequential collapse and regeneration of electrogenic pH fingerprints are associated with occupied and dynamic burrow structures, with the response time positively related to the scale of disturbance. In the case of relatively stable tube structures, built by benthos like spionid polychaetes and extending mm to cm into deposits, the electrogenic pH fingerprint is evident around the subsurface tubes. Cable filaments clearly associate with subsurface regions of enhanced solute exchange (oxidant supply) and relatively stable biogenic structures, including individual tubes and patches of tubes (e.g. made by *Sabaco*, a bamboo worm). Physically stable environments, favorable redox gradients, and enhanced organic/inorganic substrate availability promote the activity of cable bacteria in the vicinity of tubes and burrows. These findings suggest complex interactions between electrogenic activity fingerprints and species-specific patterns of bioturbation at multiple spatial and temporal scales, and a substantial impact of electrogenic metabolism on subsurface pH and early diagenetic reaction distributions in bioturbated deposits.

KEY WORDS: Sediment biogeochemistry · Cable bacteria · Bioturbation · pH dynamics · Redox micro-regions

1. INTRODUCTION

Since the concept of long-distance electron transport involving electrogenic sulfide oxidation was proposed in 2010 (Nielsen et al. 2010), the discovery of cable bacteria and the associated separation of redox reactions over distances of mm to cm, have changed traditional models of sediment diagenesis (Pfeffer et al. 2012). The geochemical consequences of cable bacteria activity — pH maxima in the oxic surface layer and minima in the deep anoxic layers — directly and indirectly influence sediment sulfur, nitrogen, oxygen, carbon, phosphorus, and iron/manganese cycling (Risgaard-Petersen et al. 2012, Rao et al. 2016, Sulu-Gambari et al. 2016a,b, van de Velde et al. 2016). The flexibility of acceptable electron donors (solid and dissolved phase sulfide) and acceptors (O_2, NO_3^-, and NO_2^-) helps explain the widespread occurrence of electrogenic sulfide oxidation. Cable bacteria are known to be active in carbonate

*Corresponding author: robert.aller@stonybrook.edu

as well as lithogenic sediments (e.g. Yin et al. 2021), and are distributed in a wide range of natural ecosystems including salt marshes, seasonally hypoxic basins, and subtidal coastal sediment environments (Malkin et al. 2014, Larsen et al. 2015, Burdorf et al. 2017), as well as in freshwater sediments (Risgaard-Petersen et al. 2015).

Electrogenic sulfide oxidation can generate a series of characteristic geochemical fingerprints, including pH distributions with sediment oxic layer maxima (cathodic oxygen reduction half reaction, $O_2 + 4e^- + 4H^+ \rightarrow 2H_2O$) and anoxic layer minima (sulfide oxidation half reaction, $½H_2S + 2H_2O \rightarrow ½SO_4^{2-} + 4e^- + 5H^+$), and wide suboxic zones (multi-cm scale) (Pfeffer et al. 2012). A recent model simulation demonstrated that the pH fingerprint can be used as a reliable indicator for the occurrence of electrogenic sulfide oxidation in both laboratory experiments and field studies (Meysman et al. 2015).

The physical structure of the cable filaments determines their vulnerability to sediment disturbance. Cable bacteria consist of multiple cells that are connected to each other within filaments which have been suggested to extend up to 7 cm in sediment deposits (van de Velde et al. 2016). There are evenly spaced ridges running along the entire length of cells in the outer membrane of filaments (Pfeffer et al. 2012, Malkin et al. 2014, Jiang et al. 2018). The ridges have been proposed to strengthen the cell–cell junction by their inherent integrity and also by incorporating strings which continuously pass through the cell–cell junctions (Jiang et al. 2018). In spite of these strengthening features, cable bacteria filaments are still fragile under unstable physical conditions. Sediment reworking by benthic organisms apparently hampers their integrity, thus inhibiting their activity fingerprints (Malkin et al. 2014). However, recent literature states that cable bacteria activity fingerprints can still be detected in bivalve reef deposits and sediments bioturbated by lugworms, and are even enhanced around solitary, stable *Chaetopterus* tubes (Burdorf et al. 2017, Malkin et al. 2017, Aller et al. 2019).

In this study, we report on investigations into the dynamics of cable bacteria activity fingerprints associated with different biogenic burrow structures in microcosms containing carbonate sediment, and the natural distributions of cable filaments in lithogenic deposits with patches of relatively stable macrofauna tubes. These 2 classes of sediments were used to evaluate the generality of the observations. Lithogenic coastal sediment was obtained from Great Peconic Bay (GPB, Eastern Long Island, New York, USA), and contained high concentrations of redox-sensitive metals (MnO_2/Mn, FeOOH/Fe) but was depleted in dissolved sulfide. Calcium carbonate-rich sediment was obtained from Florida Bay (FLB, Florida, USA), and had high dissolved sulfide but was depleted in Mn and Fe in both the solid phase and the pore water. Our goal was to examine the dynamics of electrogenic sulfide oxidation development and to relate detected geochemical fingerprints to different subsurface biogenic structures (e.g. tubes, burrows). We defined a sediment pH signal (electrogenic pH fingerprint) higher than that of seawater, due to electrogenic oxygen reduction half reaction, as the signature of electrogenic sulfide oxidation. We found that stable macrofaunal tubes could provide optimal microenvironments for cable bacteria development in subsurface sediment, as demonstrated by both subsurface electrogenic pH signals and patterns of whole and fragmented cable bacteria filament aggregations. Unstable burrows temporarily eliminated detection of local cable bacteria cathodic activity, with the recovery time of the fingerprint positively related to the scale of disturbance. Our data revealed the complex dynamics of species-specific interactions between electrogenic pH fingerprints and macrofaunal biogenic structures. Combined with earlier observations of cable bacteria aggregation in the vicinity of solitary *Chaetopterus* polychaete tubes (Aller et al. 2019), our observations suggest that electrogenic pH fingerprints and electrogenic metabolism are commonly associated with a wide spectrum of biogenic structures, and can be highly dynamic. In previous studies, a possible negative relationship between the geochemical fingerprint of electrogenic sulfide oxidation and sediment bioturbation was inferred without considering species-specific interactions more generally (Malkin et al. 2014). We conclude that because of 3D distributions and the presence of cable bacteria in bioturbated deposits, such studies likely substantially underestimated the distribution of cable bacteria filaments and their electrogenic sulfide oxidation metabolic effects.

2. MATERIALS AND METHODS

2.1. Sediment sampling

In order to evaluate the development dynamics of cable bacteria activity in the vicinity of specific biogenic structures, carbonate sediment from FLB (25.116367° N, 80.817970° W, 21°C) was collected from the upper 10 cm of mudbank deposits in Janu-

ary 2019, packed and sealed into plastic bags, and transported within 24 h to Stony Brook University. FLB is a semi-enclosed embayment with shallow water depth (<3 m). FLB mud banks and shoals are characterized by high organic matter input, high carbonate content (due to *Thalassia testudinum* deposition), and low Fe and Mn (Rude & Aller 1991, Fourqurean et al. 1992, Thamdrup 2000). The bulk sediment was stored at 4°C in the dark for 1 mo before incubation in laboratory microcosms.

To investigate the natural distributions of cable bacteria filaments in bioturbated lithogenic deposits, intact box cores of muddy sediment were collected from GPB (40.098611° N, 72.726944° W) in September 2018 and 2019. The site has a water depth of ~8 m, late summer water temperatures range from ~25 (surface) to 23°C (bottom), and salinity is ~28. The upper tier benthic community is dominated by the highly active deposit-feeding ophiuroid *Amphioplus abida*, the tube-forming maldanid polychaete *Sabaco elongatus* (10–20 cm length), and the tube-forming chaetopterid polychaete *Chaetopterus variopedatus* (parchment worm; 20–30 cm length). The mantis shrimp *Squilla empusa* is also present with ~5 cm diameter burrows extending to ~0.5–3 m (Waugh & Aller 2017) but this was avoided when sampling. Divers deployed acrylic cores (30 × 30 × 10 cm, L × H × W) to sample the top 20–25 cm of sediment along with the overlying water (salinity 28.3). Intact cores were placed in insulated coolers containing seawater from Peconic Bay, transported to Stony Brook University, NY, and held continuously aerated in the dark at the same temperature as the sampling site (23.5°C) until they were subsampled. Box cores with visible patches of S*abaco elongatus* tubes were chosen for introduction of a Br^- tracer, pore water sampling, and examination of cable bacteria distributions around tube patches. A separate box core was used to sample around individual *Sabaco* tubes. Cores were subsampled within 2–3 d of initial collection.

2.2. Cable bacteria presence and activity determination

For the FLB microcosm experiments, sediment was homogenized by sieving through a nylon mesh screen (1 mm pore) with no water added, and placed into 2 acrylic microcosms (20 × 25 × 5 cm, L × H × W) with pH and oxygen planar optical sensor sheets preinstalled onto the inner surfaces of the microcosm sides. Microcosms were filled to a depth of 10 cm with the homogenized sediment and disseminated cable bacteria (confirmed by microscope examination, described in Section 2.3.), and incubated with continuously aerated seawater at room temperature (22°C) in the dark. Overlying seawater was replaced every 3 d with fresh seawater (salinity ~25) which was collected from the West Meadow Beach (Long Island Sound, New York, USA) and filtered through 1 mm nylon mesh screen to remove particles of seagrass and algae. Parameters including pH, oxygen, H_2S, and cable bacteria filament lengths and abundances in the sediment were monitored throughout a 3 mo incubation period (pH and O_2, 2 d intervals; H_2S and bacteria abundance, 3–20 d intervals). One of the microcosms was used to study cable bacteria activity development in the vicinity of stable biogenic structures (i.e. spionid; introduced on Day 48). The other microcosm was used to study cable bacteria dynamics with mobile bioturbators (i.e. nereids; introduced on Day 80). On Day 106, both microcosms were incubated for 6 h under anoxic conditions. Anoxia with stable pH = 8.0 was attained using a mixture of N_2/CO_2 supplied through a gas proportionator. pH and H_2S distributions were imaged using planar optical sensors before and after the anoxic incubation.

For the 2018 GPB sediment, samples of cable bacteria filaments were taken on the same day as core collection at locations up against visible *Sabaco* tubes (4 subcores; tubes not sampled) and between tubes (3 subcores) using 3 ml cutoff plastic syringes (inner diameter: 8.6 mm). Syringes were inserted vertically into box cores, and the top 5 cm of the subcores were subsequently sliced at 1 cm intervals and preserved in 2% formaldehyde.

For the 2019 GPB experiment, the whole community bio-irrigation patterns were quantified by introducing the conservative tracer NaBr into water overlying a box core within 2 d after core collection. The initial Br^- concentration was 8 mM. During the tracer penetration, the box core was immersed within 1 cm of the surface in a seawater tank in the dark at the same temperature as the sampling site (22°C), and the water overlying the core was kept continuously aerated. At 24 h after tracer introduction, the core was removed from the seawater tank and the water overlying the core was collected and its volume was measured. The 4 vertical sides of the box core were replaced by inserting 4 thin plastic sheets (2 mm thickness) along the inner face. One plastic sheet had drilled grid points (2 cm spacing) to receive Rhizon pore water extractors (2 mm diameter, 5 cm length, 0.15 µm mean pore size; Rhizosphere Research Products). Rhizon extractors were inserted into each grid point perpendicular to the array planes. About 3 ml

of pore water was extracted with each Rhizon within 5 min and stored in a refrigerator for Br^- and pore water solute analyses. To ensure that there were no oxygenation artifacts, the Rhizons were first immersed in anoxic distilled water for 30 min and the first several droplets of pore water were discarded before samples were stored. Ammonia and total alkalinity were measured in addition to Br^-; however, only the Br^- concentrations are presented for interpretation of bioturbation and bioirrigation. For cable bacteria filament enumeration and length measurements, subcores were taken from the sediment by horizontally inserting 3 ml cutoff plastic syringes up to ~6.5 cm depth at the same locations as the Rhizon ports on a vertical array plane, and were immediately preserved in 2% formaldehyde.

2.3. Analytical methods

The length of filaments and number of cells in the filaments were enumerated from acridine orange (AO)-stained samples under epifluorescence microscopy, with cable bacteria identified by their unique filament morphology. We assumed a minimum filament length to have at least 3 connected cells. The total lengths of filaments in a given depth interval was converted into filament cell abundances based on an averaged cell length of 2 µm. Cable bacteria filament identity was also confirmed by fluorescence *in situ* hybridization (FISH) with a Desulfobulbaceae-specific oligonucleotide probe (DSB706; 5′-ACC CGT ATT CCT CCC GAT-3′) (Manz et al. 1992). The detailed procedure of filament enumeration is described elsewhere (Aller et al. 2019).

Br^- was measured in triplicate on 20 µl samples using a modified 96-well plate spectrometric method adapted from the phenol red-bromophenol blue method (Lepore & Barak 2009).

The pH imaging planar optical sensor was modified after Zhu et al. (2005), based on 8-hydroxy-1,3,6- pyrenetrisulfonic acid trisodium salt (HPTS) as a pH indicator. Oxygen-sensing membranes were made with platinum tetrakis(pentafluorophenyl)porphyrin (Lee & Okura 1997). H_2S sensors were made using diphenylcarbazone-Zn as an indicator (Yin et al. 2017). Two-dimensional (2D) pH sensor membrane images were taken using a commercial Canon camera (EOS Rebel T7i) under excitation light at 510 and 430 nm wavelengths and with the emission wavelength fixed at 545 nm. The numerical ratios of the 2 emission images were calculated to make calibrations against standard strip membranes. The pH distribution was calibrated using NBS scale Tris-HCl buffers, and pH data reported here are on the NBS scale. Oxygen concentrations were calibrated based on the Stern-Volmer relationship (Lee & Okura 1997) with sensor emissions at 650 nm captured after 395 nm excitation using the same camera system. H_2S sensor responses were recorded using a flatbed scanner (Canoscan 8400F) and calibrated using sensor strip standards exposed to known H_2S concentrations for identical times. All 2D sensor image data were also converted to 1D vertical profiles by horizontal averaging of vertically oriented membranes (widths ~0.5 cm).

3. RESULTS

3.1. Subsurface stable biogenic structures promote cable bacteria activity fingerprint

In the case of the 2 FLB microcosms, sediment surface pH maxima indicating electrogenic sulfide oxidation gradually developed after 20 to 22 d, with pH reaching 8.4 to 8.5 (data not shown). Hydrogen sulfide dynamics and bacterial abundances also confirmed that electrogenic sulfide oxidation was well developed and active until the end of the incubation period (Day 106) (see Fig. S3 in the Supplement at www.int-res.com/articles/suppl/m669p051_supp.pdf).

After a ~2 cm long spionid polychaete was introduced into 1 of the microcosms on Day 48, its burrowing and search behavior immediately inhibited the detection of electrogenic pH fingerprints in the vicinity of its activities. In contrast, when a stable tube (mm scale outer diameter [OD], sub-cm scale length) was constructed by Day 65, an electrogenic pH fingerprint gradually developed in the vicinity of the tube (Fig. 1). Before stable tubes were built, a spot with low pH formed, breaking an otherwise continuous pH maximum band at the sediment surface on Day 48. By Day 52, the size of the low pH area enlarged to ~1 cm associated with bioturbation by the spionid. From Day 52 to 56, a continuous pH maximum band regenerated on the sediment surface, due to either a lack of burrowing or movement of the worm away from the image plane. Because of tube-construction and subsequent feeding activity, a more complex pH distribution began to develop on Day 65. A lumen-shaped, high pH fingerprint associated with a tube also gradually built up from Day 65 to 76. Since the tubes were not immediately against the microcosm image plane, the pH signal was from pore water affected by spionid irrigation, local redox reac-

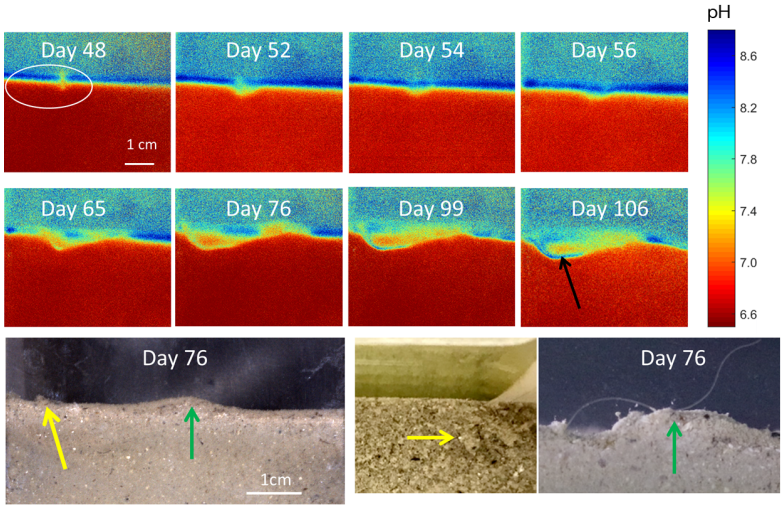

Fig. 1. The 2D pH dynamics of the spionid polychaete-inhabited microcosm with visible light images showing the tube position. Top: 2D pH dynamics. On Day 48, a spionid can be seen actively searching for a suitable location. The burrowing behavior affected the fingerprints of electrogenic sulfide oxidation. The breakage and reconnection of the pH maxima (from Day 48 to 56) can be observed as burrow activity appears and disappears from the image plane. After a stable tube was established, the electrogenic pH fingerprint developed in subsurface sediment around the oxic conduits (black arrow, also see Fig. 2). Bottom: visible light images (position as indicated by the white circle in the pH figure). The small mounds on the sediment surface (yellow and green arrows) indicate the locations of the spionid burrows. The middle close-up image of the surface shows 2 tubes, indicated by a yellow arrow, extending from the sediment into the overlying water. The extended part of the tube is not immediately against the plane of the microcosm. The right close-up image shows movement of the spionid tentacles (green arrow)

tions, and cable bacteria activity. Due to the constant bioturbation of the spionid on the sediment surface, sediment kept being disturbed locally without re-establishment of pH maxima. However, electrogenic sulfide oxidation was still happening elsewhere, as reflected by stable elevated pH signals in the microcosm away from spionid burrows. When the spionid tube was stabilized, subsurface pore water pH around the tube lumen gradually increased from Day 76 to 106 with the highest pH of ~8.5 detected at 0.9 cm depth (Figs. 1 & 2). The subsurface pH elevations showed great spatial variability (Fig. 2C, prior to anoxia).

3.2. Mobile bioturbators inhibit cable bacteria activity fingerprint

Juvenile nereids were introduced into the second FLB sediment microcosm during replacement of the overlying water. On Day 80, a vertical polychaete burrow (~0.5 mm OD) at ~1.5 cm depth was evident from the visible image on the pH optode monitoring side, but it did not extend to the sediment surface along the image plane (Fig. 3). No pH disturbance associated with bioturbation was found in anoxic sediment and the electrogenic pH fingerprint still persisted immediately above the burrow. From Day 83, consistent with ongoing burrow construction and irrigation, subsurface pH was elevated to 7–7.4 around the burrows. On Day 84, with the burrow open to the overlying water, the pH maximum band at the sediment–water interface became discontinuous. On Day 86, the sediment surface end of the burrow was closed, suggesting that the polychaete was no longer inhabiting it, and the pH returned to 8.5 at the image plane. On Day 87, however, the previously abandoned burrow was re-inhabited, with low pH (pH ~7) in the burrow area reflecting the exchange with low pH anoxic pore water. Over the next 13 h, the burrow was abandoned again, and the surface opening was closed. This was followed by the regeneration of an activity signal from electrogenic sulfide oxidation in the surface sediment with an abandoned burrow structure ~0.5 cm underneath. Pore water pH in the abandoned burrow lumen decreased to 6.5 at the same time.

In addition to vertical burrow sections, nereids can also make horizontal burrows (Fig. 4). Horizontal burrows with approximately 0.8 and 0.5 cm lengths were identified on the pH monitoring side on Day 96. The burrows were near the oxic–anoxic interface (~2 mm depth) and cut across the vertical pathways of cable bacteria electron transport. The corresponding pH pattern showed that local sediment surface pH decreased to around 6.8–7.8. After Day 99, the horizontal burrows were abandoned and closed, and the pH maximum band regenerated gradually but did not reconnect until Day 105, slower than the recovery time observed with vertical burrows. The impacts of sediment reworking by nereids are highly dynamic and depend on the orientation of burrows relative to an oxic interface and on scale. From Day 99 to 105, against the plane of the microcosm, burrow conduits through the side of the microcosm were continuously generated, inhabited, and subsequently abandoned, coinciding with oscillations of pore water pH in the vicinity of irrigated or abandoned burrows.

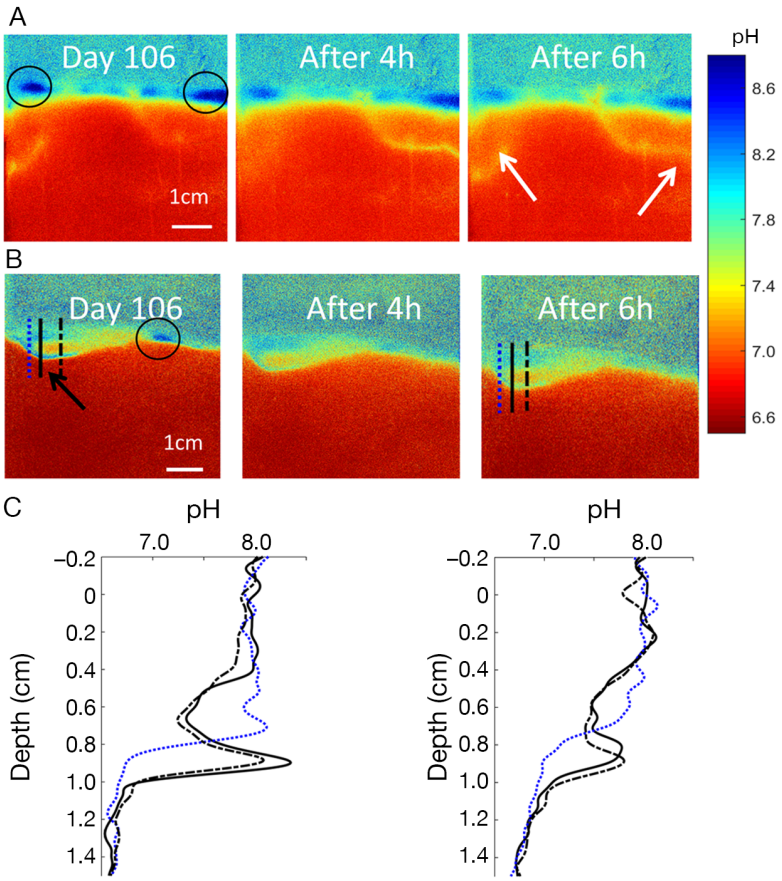

Fig. 2. The 2D and 1D pH dynamics during 6 h of overlying water anoxia, and the disappearance of sediment surface (black circles)/subsurface (black vertical lines) pH maxima. (A) pH dynamics in the microcosm with nereid burrows (white arrows). The nereid microcosm showed higher sediment surface pH values compared with the spionid microcosm prior to deoxygenation. After 6 h of anoxia, sediment surface pH decreased and pH at depth changed only slightly. pH values in the vicinity of relic nereid burrow areas still had high pH (~7). (B) pH dynamics in the microcosm with a spionid tube (black arrow). Sediment surface pH maxima had almost completely disappeared after 4 h anoxia and the subsurface pH maxima around the spionid tube had almost completely disappeared after 6 h. (C) The 1D pH distributions in the spionid microcosm with oxic overlying water and after a 6 h period of anoxia. The 1D profiles are plotted at different locations relative to a spionid tube by horizontal averaging of vertically oriented membranes (widths ~0.07 cm), with the color codes in the 2D images matching those in the 1D profiles. Under oxic conditions, pH distributions in the vicinity of the tube are more heterogeneous, and a subsurface pH maxima (~8.5) was observed at a 0.9 cm depth along the burrow wall. After 6 h anoxic incubation, the spatial heterogeneity of the subsurface pH diminished

The oxic layer sediment was locally removed on one side of the microcosm during the replacement of the overlying water, as illustrated by a visible light photograph taken on Day 63 (Fig. S1 in the Supplement). Before sediment disturbance, the sediment surface pH maximum band was continuous. Right after the disturbance, the pH dropped to 7.4–7.8 at the site where the oxic sediment layer was completely removed. Complete recovery of the pH maxima band following the disturbance took about 20 d (Day 80).

3.3. Cable bacteria activity dependent on O_2

On Day 106, the overlying water of FLB sediment microcosms was switched from oxic to anoxic for 6 h to check for the cessation of the biogeochemical response of electrogenic sulfide oxidation. Prior to overlying water anoxia, the sediment surface pH maxima were still detectable in the 2 replicate microcosms. The build-up of H_2S and a corresponding decrease in sediment surface pH in the spionid microcosm suggest, however, that electrogenic sulfide oxidation had diminished in undisturbed areas relative to earlier stages (Figs. 1 & S3). After the overlying water had been deoxygenated with a N_2/CO_2 mixture (overlying water pH ~8.0; no O_2 detected), the sediment surface pH maxima decreased in the nereid microcosm (6 h after anoxia), and almost completely disappeared in the spionid microcosm (4 h after anoxia) (Figs. 2 & S3). The 2D pH distribution showed highly heterogeneous pH patterns at the upper surface in the nereid microcosm with hotspots of high pH even after the 6 h anoxic incubation. Anoxic sediment pH changed slightly. In contrast, H_2S either did not change significantly or expanded only slightly in the 2 microcosms (Fig. S3).

The subsurface pH values in the vicinity of nereid burrow structures were nearly constant during the 6 h of anoxia. Two nereid burrows were found on Day 106 during anoxia, and the pH remained relatively high near the relic burrows compared with the surrounding sediment (7.5 vs. 6.5) (Fig. 2). In the spionid microcosm, the elevated pore water pH associated with a spionid tube in the subsurface sediment decreased from 8.5 to 8.0 during the 6 h anoxic period, and the pH vertical profiles showed less spatial variability at different locations relative to the lumen. The pH elevation signa-

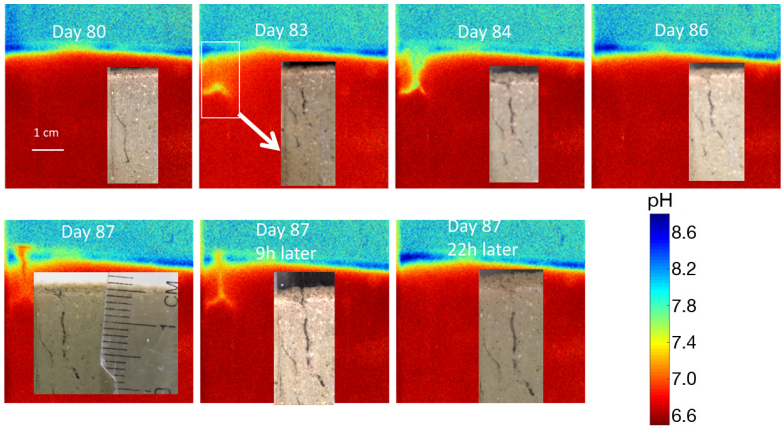

Fig. 3. The 2D pH dynamics of the microcosm containing nereids (ragworms) with visible light images showing burrow dynamics. Top: pH dynamics. On Day 80, the pH signals of electrogenic sulfide oxidation were well developed. From Day 83 to 87, nereid burrows developed on the left side of the microcosm which affected electrogenic pH fingerprint. Visible light image inserts show the scales of the burrow. The vertical burrow extended to 1.5 cm depth with an OD of ~0.5 mm. The surface end of the burrow was open (Days 84 and 87) or closed (Days 80, 83, and 86) depending on nereid activity

tures around relic burrows were still detectable in both of the microcosms after 6 h of anoxia; however, this does not necessarily mean that the animals were still alive and active. It is possible that passive irrigation of burrow structures occurred during aeration/circulation of the overlying water with the N_2/CO_2 mixture, resulting in the transport of relatively high pH water though tubes and burrows.

3.4. Cable bacteria aggregations in the vicinity of stable biogenic structures

In the 2019 GPB whole-community experiment, the Br^- tracer penetrated through a depth of 10 cm within 24 h in the middle of the box core, creating heterogeneous tracer distributions (Fig. 5). *Sabaco* tubes were located over the Rhizon array positions at 14 to 18 cm along the *x*-axis and 0 to 10 cm along the *y*-axis, ranges being inferred from sediment surface morphology, core dissection following Rhizon sampling, and the tracer penetration patterns. Cable bacteria filaments (3 to 90 cells) were heterogeneously distributed in the sediment. Aggregations of filaments with at least 3 cells were maximal near the perimeter of the *Sabaco* tube patch. Free bacteria cells were also unevenly distributed in the subsurface sediment, with highest abundances found in the vicinity of cable bacteria filament cell aggregations.

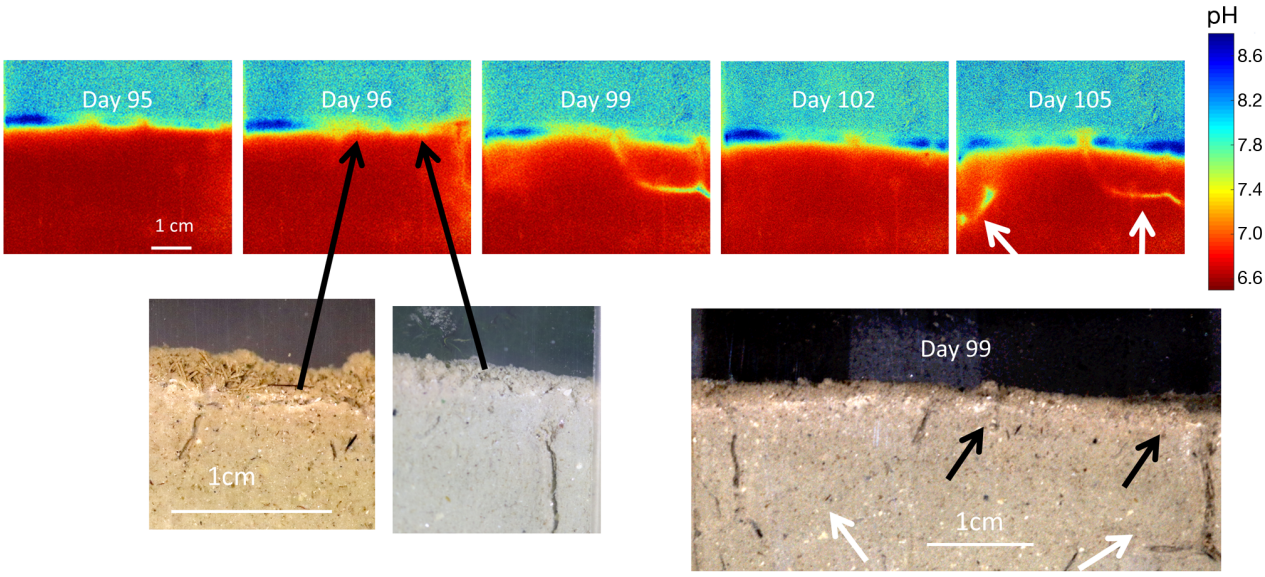

Fig. 4. The 2D pH dynamics of the microcosm containing nereids (ragworms) with visible light images showing the positions of burrows (scales vary). Top: pH dynamics. Burrows (0.5 and 0.8 cm long; black arrows) were discovered near the oxic–anoxic sediment interface on Day 96 associated with the disappearance of the local sediment surface pH maxima. The horizontal burrows were abandoned on Day 99 and the pH fingerprints recovered slowly with clear pH maxima appearing by Day 105. Bottom: visible light images showing the dimensions and positions of the 2 horizontal nereid burrows (black arrows). Two other vertical burrows are visible on the left and right edges on Days 99 and 105 (white arrows) (see also Fig. 2)

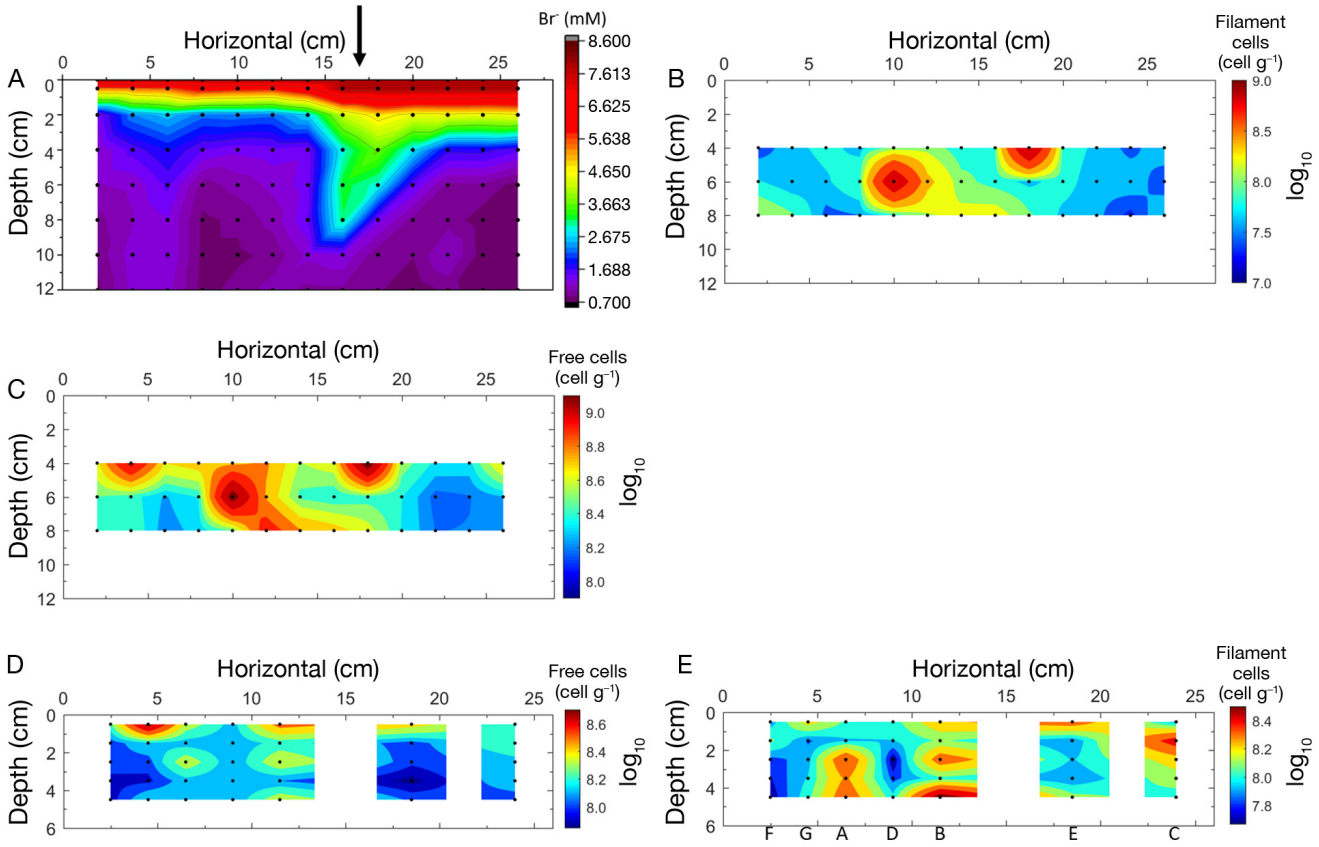

Fig. 5. The 2D Br^-, filament cell, and bacteria free cell distributions in (A,B,C) the whole-community 2019 Great Peconic Bay (GPB) core and (D,E) in the 2018 GPB core. An aggregation of *Sabaco* tubes was observed at 15 to 20 cm along the *x*-axis of 2019 GPB (black arrow). (A) The 2D Br^- tracer penetration pattern. A high concentration Br^- tongue was observed within 14 to 18 cm along the *x*-axis and 0 to 8 cm along the *y*-axis. (B) Distribution of cable bacteria filament cells with aggregations around *Sabaco* tube patches. (C) Bacteria free cell distribution. The locations with high abundance coincide with zones of deeper tracer penetration. (D) Bacteria free cell distribution in 2018 GPB. (E) Cable bacteria filament cell distribution. More filament cells were found aggregated in the subsurface sediment in the vicinity of *Sabaco* tubes. Filament cell abundances were low in locations where no tubes were observed (sample locations F, G, A, D, B, E, C indicated at base of *x*-axis). An overhead view visible light image of the core is shown in Fig. S2

Distinct patterns of bacterial abundance were found in the 4 subcores oriented immediately against *Sabaco* tubes and the 3 subcores between tubes (Figs. 5 & S2). At locations A, B, C, and F, where subcores were taken against *Sabaco* tubes, cable bacteria filaments (3 to 55 cells) were enriched in the subsurface layers at different depths and depleted in the surface sediment. At other locations between *Sabaco* tubes (locations G, D, and E), cable bacteria filament cell abundances were generally lower. However, in contrast to the samples collected near the tubes, the most abundant cable bacteria filament cell sections were found in the surface layers in samples away from tubes. As found in the 2019 GPB box core, the abundance of bacteria free cells was positively correlated with the numbers of cable bacteria filament cells.

4. DISCUSSION

4.1. Redox boundary: aggregation and activity of cable bacteria in the vicinity of irrigated biogenic structures

As demonstrated by the correspondence between Br^- tracer penetration and bacterial abundances, filamentous cable bacteria clearly associate with regions of deposits characterized by rapid solute exchange with overlying water (Fig. 5). Small-scale, oriented sampling also showed directly that filaments are present at low abundances throughout deposits, but they are more abundant in the vicinity of subsurface *Sabaco* tubes. Such association has been observed for both patches of relatively small tubes (mm OD), as shown here in the case of the maldanid *Sabaco*, as

well as larger (cm OD), solitary tubes, as found for the parchment worm *Chaetopterus* (Aller et al. 2019). The enhanced and predictable exchange of pore water solutes with overlying water by the ventilated tube structures at both individual and patch scales supplies O_2 directly and stimulates nitrification (NO_3^- production) in tube walls (Aller 2001, Kristensen & Kostka 2005), creating high-level oxidant redox domains and favoring cathodic reduction reactions by cable bacteria.

Subsurface redox domains for cable bacteria clusters are not solely restricted to biogenic structures formed by marine polychaetes, plant rhizospheres can also provide similar redox conditions by leaking oxygen through roots into sulfidic sediments. Cable bacteria have been found to be enriched near plant rhizosphere oxic–anoxic transition zones along with a radial orientation of filaments next to the roots (Martin et al. 2019; Scholz et al. 2019). The results from the present and previous studies, make it clear that in nature, cable bacteria aggregate around a variety of subsurface stable redox microenvironments with widely variable dimensions.

In this study, the vertical cable bacteria abundance patterns also showed that cable bacteria aggregated in the sediment subsurface near *Sabaco* tubes but were also enriched in the surface layer away from tubes (Fig. 5). The 2 different patterns may be the result of the feeding activity of *Sabaco* in the surface sediment (e.g. hoeing behavior) (Levin et al. 1997). Numbers of nematodes, which likely graze cable bacteria, at the Great Peconic Bay site were also higher in the surface sediment than at depth (Aller et al. 2019), which may contribute to cable bacteria being more aggregated in the subsurface sediment near the tube than anywhere else in the surface sediment.

The development dynamics of the electrogenic sulfide oxidation fingerprint surrounding spionid tubes in the carbonate sediment demonstrated the tube–cable bacteria interaction. The tube-building macrofauna in these sediments have different effects on the electrogenic pH fingerprint, inferring electrogenic sulfide oxidation, at different stages of tube construction. At the start of spionid tube formation, the geochemical fingerprint of electrogenic sulfide oxidation was inhibited, as reflected by the break up and dynamic reconnection of the continuous sediment surface pH maxima band. After stable tubes were built (Day 65), the anoxic sediment was irrigated with overlying water and pore water pH increased (Fig. 1). Bioturbation had only local effects, and the electrogenic pH fingerprint was not affected in the locations not directly disturbed by spionid burrowing. After formation, the continuously irrigated tube provided a stable redox microenvironment suitable for electrogenic sulfide oxidation below the sediment–water interface (Figs. 1 & 2). The subsurface pH elevation can only be explained by electrogenic sulfide oxidation with the cathode terminus oriented towards the spionid tube. However, the spatial heterogeneity of elevated pH does not necessarily mean that there was heterogeneity in the electrogenic sulfide oxidation in the stable redox microenvironment around the tube. Because the position of the spionid tube was not necessarily equidistant from the planar sensor, and other redox reactions (e.g. aerobic oxidation, sulfate reduction) can diminish the pH elevation signals, the spatial variations in pH vertical profiles could simply be due to variations in the distance from the actual tube.

It is clear that a stable redox boundary is necessary for subsurface electrogenic sulfide oxidation. Once the redox gradient is eliminated, the electrogenic pH fingerprint declines, indicating the decline of electrogenic sulfide oxidation. During overlying water anoxia, sediment surface pH elevations in the 2 FLB microcosms decreased gradually (Fig. 2). The subsurface pH maxima in the vicinity of a spionid tube also decreased to the seawater value. These responses suggest that the original pH maxima signal in both of the microcosms were caused by cable bacteria electrogenic activity, and the irrigation with overlying oxic water promoted subsurface electrogenic sulfide oxidation. Our data also showed different pH responses to anoxia in the 2 microcosms, with the sediment surface pH maxima diminished in one microcosm but almost completely absent in the other after 6 h of anoxia (Figs. 2 & S3). We believe the different pH response dynamics in the 2 microcosms were due to the initially lower electrogenic sulfide oxidation in the spionid microcosm on Day 106, which showed a weaker sediment surface pH elevation prior to anoxic incubation, and the depth of detectable H_2S had also shoaled to 0.75 cm (Fig. S3). Previous studies have also shown that electrogenic sulfide oxidation declines after extended incubation (Schauer et al. 2014). The slow disappearance rate of pH fingerprints in the nereid microcosm is likely due in part to carbonate mineral dissolution buffering proton accumulation. In addition, the H_2S distribution did not change very much after the anoxic incubation period compared with previous published data obtained during a similar time interval (Nielsen et al. 2010).

4.2. Physical stability: scale and dynamics of bioturbation impact on electrogenic pH fingerprint

As illustrated by the response of the electrogenic pH fingerprint to redox oscillations, physical stability is advantageous but not an absolute requirement for the development of filamentous cable bacteria and electrogenic activity. The electrogenic pH fingerprint is affected significantly by highly mobile, juvenile nereid polychaetes. The bioturbation behavior of nereids may cause the breakdown of cable bacteria filament integrity (Pfeffer et al. 2012), terminating the electrogenic sulfide oxidation reaction. The increased sediment mixing and solute transport processes brought about by bioturbation can also hamper the detection of electrogenic pH fingerprints (Yin et al. 2021). The regeneration of an electrogenic pH fingerprint is quite dynamic. In the case of carbonate muds, when a burrow is abandoned and its opening to the sediment surface is closed, an electrogenic pH signal can be quickly regenerated within 13 h (Fig. 3). The time scale of activity fingerprint regeneration and the relative position of the abandoned burrow possibly indicate the spread of nearby filaments from the surface sediment, the migration of filaments in the anoxic sediment to the surface overlying the abandoned empty burrow, or the expression of the sediment surface pH fingerprint due to diffusion. The spreading and migration mechanisms are mechanistically possible because of the mobility and flexibility of the cable bacteria filaments (Bjerg et al. 2018, Jiang et al. 2018). The spreading and overlying mechanisms during electrogenic reaction recovery suggest that filaments are more correctly depicted as a network. We also observed that the proportion of burrow extending into anoxic sediment that is either actively bio-irrigated or not will not affect the sediment surface pH maximum signals (Figs. 2, 3 & 4), suggesting that the cable bacteria filament anodic ends may be distributed over a range of depths. Before the formation of spionid tubes in the other microcosm, the bioturbation activity of the tube-building species negatively affected the signature of cable bacteria activity (Fig. 1). After the formation of subsurface biogenic structures, the feeding activity of spionids in the surface sediment also negatively interfered with the local electrogenic pH fingerprint.

Clearly, the recovery rate of electrogenic pH fingerprints is directly proportional to the scale of bioturbation. Under mm scale disturbance (i.e. nereid vertical burrows), the sediment surface pH maxima were re-established within ~13 h after the burrow was abandoned. Under cm scale disturbance (i.e. nereid horizontal burrows at the oxic–anoxic sediment interface), it took up to 10 d to recover. When the whole oxic layer was removed (i.e. disturbance by an aerator), the sudden collapse of the electrogenic sulfide oxidation fingerprint and the exposure of low pH anoxic sediment decreased sediment surface pH. After the exposed anoxic sediment was oxidized, the electrogenic sulfide oxidation fingerprint re-established at the newly formed stable redox environment in around 20 d (Fig. S1), which is about the same time as that required for detection of sediment pH maxima after microcosms were setup.

In natural sedimentary environments, physically stable redox domains are restricted by mobile sediment bioturbators, and it has been thought that the geochemical fingerprint of electrogenic sulfide oxidation would be deleteriously affected (Malkin et al. 2014). More recent studies, however, have demonstrated that electrogenic sulfide oxidation can coexist and be active in the presence of macrofauna, including in deposits inhabited by bivalves, polychaetes, and mud shrimp (Burdorf et al. 2017, Malkin et al. 2017, Li et al. 2020). Instead of a simple negative relationship between bioturbation and cable bacteria electrogenic activity fingerprints, effects are clearly more nuanced and depend on relative time and spatial scales of disturbance and filament colonization, that is, the interaction between redox domain residence times and microbial fingerprint response times. Our studies suggest mobile and tube-building benthos have complex, dynamic effects on local cable bacteria activity fingerprints that can be both positive and negative (see also data of Hermans et al. 2019). The resulting highly heterogeneous cable bacteria activity fingerprint might be readily overlooked when making inferences from sparse 1D microelectrode measurements alone.

4.3. Substrate availability: an additional explanation for filament aggregation

Single or free bacteria cells aggregate in the same subsurface regions as cable bacteria filaments. Fig. 5B,C shows that cable bacteria filament cells and free cells were clearly elevated around the *Sabaco* tubes, but the distributions were heterogeneous. Similar distribution patterns of free cell bacteria have been observed around *Chaetopterus* tubes in GPB (Aller et al. 2019), and an increase in the numbers of bacteria is a generally observed pattern around burrows (Kristensen & Kostka 2005). The enhanced bac-

teria free cell distributions around macrofauna tubes might be caused by the promotion of microbial metabolism due to stimulated oxic and suboxic reactions around burrows (Zhu et al. 2006a,b). Additional labile organic substrates can be present around tubes and burrows, although the tubes of infauna such as the burrowing anemone *Ceriantheopsis* and the polychaete *Chaetopterus* are generally refractory relative to fresh labile planktonic material (Kristensen et al. 1991). However, the organic matter at ambient sediment depths of 10 to 12 cm might be more refractory than the *Chaetopterus* tubes themselves. Thus, a tube lining could promote the formation of subsurface bacteria hotspots. Under some circumstances, cable bacteria metabolic activity has been shown to be heterotrophic (Vasquez-Cardenas et al. 2015). However, more recent studies have shown that cable bacteria may be autotrophic (Kjeldsen et al. 2019, Geerlings et al. 2020). In either case, the more labile organic matter and nutrients around burrows and tubes could promote cable bacteria aggregation. Based on cable bacteria filament cell distribution patterns such as those reported here and also by Reimers et al. (2017) and Aller et al. (2019), electrogenic reaction is likely to be just one of the multiple metabolic pathways for cable bacteria to conserve energy, suggesting they have the potential to carry out other metabolic activities that do not require stable redox domains. This means that the factors contributing to the aggregation of cable bacteria in the vicinity of stable biogenic structures may be the same as for free bacteria cells. In the vicinity of plant rhizospheres, the formation of cable bacteria filament aggregations can be promoted by organic substrates secreted from roots that also leak oxygen (Martin et al. 2019, Scholz et al. 2019). It seems reasonable that enhanced formation of filaments around biogenic sedimentary structures and roots reflects a direct heterotrophic requirement (Vasquez-Cardenas et al. 2015) and/or an indirect requirement through interaction with SO_4^{2-} reducers (sulfide source) or other components of the consortia necessary to sustain electrogenic metabolism (Lovley 2017).

The occurrence of long distance electron transport metabolism distinguishes cable bacteria from other bacteria, and their electrogenic metabolic activity significantly affects sediment early diagenetic reactions (Pfeffer et al. 2012, Rao et al. 2016). The biogeochemical significance of filament aggregations diminishes if cable bacteria do not carry out electrogenic sulfide oxidation in natural environments. Therefore, electrogenic metabolic activity or the geochemical fingerprints of it must be directly tested to evaluate cable bacteria activity relative to the range of redox domains associated with biogenic struc-

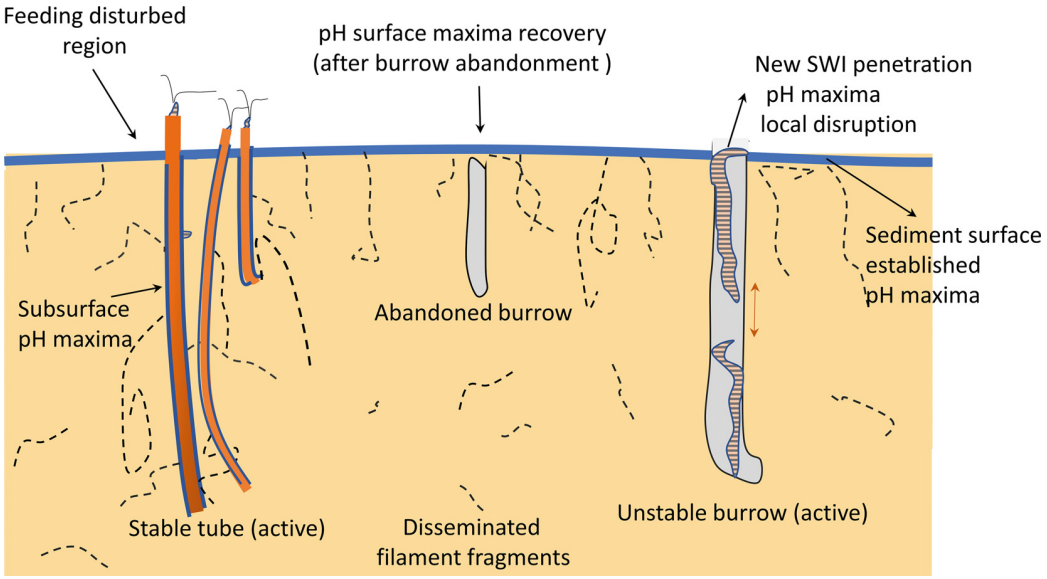

Fig. 6. Schematic of electrogenic sulfide oxidation and cable bacteria interactions. Cable bacteria distribute unevenly in sediments, aggregating around sediment subsurface stable redox domains (e.g. tubes) and elevating localized pore water pH at oxic boundaries (sediment surface and subsurface oxic boundaries are shown as blue). Networks of filaments may characterize stable domains. Actively inhabited unstable burrows inhibit the establishment of electrogenic pH fingerprints, breaking the continuity of the pH maximum band at the sediment surface (a 2D view) and creating complex pH distributions. The dynamics of electrogenic sulfide oxidation fingerprints are modified by local bioturbation activities. Once burrows are abandoned, the activity fingerprints recover within hours to days, depending on the scales (mm to cm) of initial disturbance. SWI: sediment–water interface

tures. Currently available methods such as electric potential microelectrode, pH microelectrode, and optical sensors may be promising for the study of cable bacteria activity signatures in such microenvironments (Zhu et al. 2005, Damgaard et al. 2014).

5. CONCLUSIONS

Cable bacteria activity affects sediment biogeochemical cycling through remotely coupled oxygen, nitrate, and nitrite reduction in oxic surface sediment with sulfide oxidation at depth. The characteristic pH distributions generated during cable bacteria activity indirectly impact multiple elemental cycles. In this study, we provide direct evidence for the aggregation of cable bacteria around relatively stable biogenic structures at individual and patch scales in lithogenic sediment, indicating that abundances of cable bacteria can be enhanced around a variety of stable biogenic structures even with different substrates, dimensions, and residence times in nature (Fig. 6). The dynamics of electrogenic pH fingerprint development in the vicinity of biogenic structures of mm diameter and cm length scales (nereid burrows, spionid tubes) were studied during different stages of burrow formation. With the rapid detection of an electrogenic sulfide oxidation signal after the construction of spionid tubes (days to weeks), our data imply that in previous studies, the distributions of electrogenic sulfide oxidation geochemical fingerprint were underestimated because of an emphasis on 1D vertical patterns near the upper sediment. Physical stability, redox gradients, and substrate availability promote the development of electrogenic pH fingerprints in subsurface sediment. Bioturbation in sediment clearly has a complex spectrum of local impacts on early diagenetic reactions due to both positive and negative interactions with cable bacteria and their associated fingerprints, which depend on different burrow features and macrofaunal growth stages that affect electrogenic sulfide oxidation differently.

Data availability. All the data that support the findings of this study are available from the corresponding author upon reasonable request.

Acknowledgements. We thank W. Cong, Z. Qi, and C. Heilbrun for assistance in the field and laboratory, and B. Furman (Florida Fish and Wildlife Conservation Commission) for collecting sediment samples for this study. We thank Sebastiaan van de Velde and 2 anonymous reviewers for providing helpful comments. This work was supported by NSF OCE 1737749 and NSF OCE 1332418.

LITERATURE CITED

Aller RC (2001) Transport and reactions in the bioirrigated zone. In: Boudreau BP, Jorgensen BB (eds) The benthic boundary layer. Oxford University Press, Oxford, p 269–301

Aller RC, Aller JY, Zhu Q, Heilbrun C, Klingensmith I, Kaushik A (2019) Worm tubes as conduits for the electrogenic microbial grid in marine sediments. Sci Adv 5: eaaw3651

Bjerg JT, Boschker HT, Larsen S, Berry D and others (2018) Long-distance electron transport in individual, living cable bacteria. Proc Natl Acad Sci USA 115:5786–5791

Burdorf LD, Tramper A, Seitaj D, Meire L and others (2017) Long-distance electron transport occurs globally in marine sediments. Biogeosciences 14:683–701

Damgaard LR, Risgaard-Petersen N, Nielsen LP (2014) Electric potential microelectrode for studies of electrobiogeophysics. J Geophys Res Biogeosci 119:1906–1917

Fourqurean JW, Zieman JC, Powell GV (1992) Phosphorus limitation of primary production in Florida Bay: evidence from C:N:P ratios of the dominant seagrass *Thalassia testudinum*. Limnol Oceanogr 37:162–171

Geerlings NM, Karman C, Trashin S, As KS and others (2020) Division of labor and growth during electrical cooperation in multicellular cable bacteria. Proc Natl Acad Sci USA 117:5478–5485

Hermans M, Lenstra WK, Hidalgo-Martinez S, van Helmond NA and others (2019) Abundance and biogeochemical impact of cable bacteria in Baltic Sea sediments. Environ Sci Technol 53:7494–7503

Jiang Z, Zhang S, Klausen LH, Song J and others (2018) In vitro single-cell dissection revealing the interior structure of cable bacteria. Proc Natl Acad Sci USA 115:8517–8522

Kjeldsen KU, Schreiber L, Thorup CA, Boesen T and others (2019) On the evolution and physiology of cable bacteria. Proc Natl Acad Sci USA 116:19116–19125

Kristensen E, Kostka JE (2005) Macrofaunal burrows and irrigation in marine sediment: microbiological and biogeochemical interactions. In: Kristensen E, Haese RR, Kostka JE (eds) Interactions between macro- and microorganisms in marine sediments. Coastal and estuarine studies, Vol 60. American Geophysical Union, Washington, DC, p 125–157

Kristensen E, Aller RC, Aller JY (1991) Oxic and anoxic decomposition of tubes from the burrowing sea anemone *Ceriantheopsis americanus*: implications for bulk sediment carbon and nitrogen balance. J Mar Res 49:589–617

Larsen S, Nielsen LP, Schramm A (2015) Cable bacteria associated with long-distance electron transport in New England salt marsh sediment. Environ Microbiol Rep 7: 175–179

Lee SK, Okura I (1997) Photostable optical oxygen sensing material: platinum tetrakis(pentafluorophenyl)porphyrin immobilized in polystyrene. Anal Commun 34:185–188

Lepore BJ, Barak P (2009) A colorimetric microwell method for determining bromide concentrations. Soil Sci Soc Am J 73:1130–1136

Levin L, Blair N, DeMaster D, Plaia G, Fornes W, Martin C, Thomas C (1997) Rapid subduction of organic matter by maldanid polychaetes on the North Carolina slope. J Mar Res 55:595–611

Li C, Reimers CE, Chapman JW (2020) Microbiome analyses and presence of cable bacteria in the burrow sediment of *Upogebia pugettensis*. Mar Ecol Prog Ser 648:79–94

Lovley DR (2017) Happy together: microbial communities that hook up to swap electrons. ISME J 11:327–336

Malkin SY, Rao AM, Seitaj D, Vasquez-Cardenas D and others (2014) Natural occurrence of microbial sulphur oxidation by long-range electron transport in the seafloor. ISME J 8:1843–1854

Malkin SY, Seitaj D, Burdorf LD, Nieuwhof S and others (2017) Electrogenic sulfur oxidation by cable bacteria in bivalve reef sediments. Front Mar Sci 4:28

Manz W, Amann R, Ludwig W, Wagner M, Schleifer KH (1992) Phylogenetic oligodeoxynucleotide probes for the major subclasses of proteobacteria: problems and solutions. Syst Appl Microbiol 15:593–600

Martin BC, Bougoure J, Ryan MH, Bennett WW and others (2019) Oxygen loss from seagrass roots coincides with colonisation of sulphide-oxidising cable bacteria and reduces sulphide stress. ISME J 13:707–719

Meysman FJ, Risgaard-Petersen N, Malkin SY, Nielsen LP (2015) The geochemical fingerprint of microbial long-distance electron transport in the seafloor. Geochim Cosmochim Acta 152:122–142

Nielsen LP, Risgaard-Petersen N, Fossing H, Christensen PB, Sayama M (2010) Electric currents couple spatially separated biogeochemical processes in marine sediment. Nature 463:1071–1074

Pfeffer C, Larsen S, Song J, Dong M and others (2012) Filamentous bacteria transport electrons over centimetre distances. Nature 491:218–221

Rao AM, Malkin SY, Hidalgo-Martinez S, Meysman FJ (2016) The impact of electrogenic sulfide oxidation on elemental cycling and solute fluxes in coastal sediment. Geochim Cosmochim Acta 172:265–286

Reimers CE, Li C, Graw MF, Schrader PS, Wolf M (2017) The identification of cable bacteria attached to the anode of a benthic microbial fuel cell: evidence of long distance extracellular electron transport to electrodes. Front Microbiol 8:2055

Risgaard-Petersen N, Revil A, Meister P, Nielsen LP (2012) Sulfur, iron-, and calcium cycling associated with natural electric currents running through marine sediment. Geochim Cosmochim Acta 92:1–13

Risgaard-Petersen N, Kristiansen M, Frederiksen RB, Dittmer AL and others (2015) Cable bacteria in freshwater sediments. Appl Environ Microbiol 81:6003–6011

Rude PD, Aller RC (1991) Fluorine mobility during early diagenesis of carbonate sediment: an indicator of mineral transformations. Geochim Cosmochim Acta 55:2491–2509

Schauer R, Risgaard-Petersen N, Kjeldsen KU, Bjerg JJT, Jørgensen BB, Schramm A, Nielsen LP (2014) Succession of cable bacteria and electric currents in marine sediment. ISME J 8:1314–1322

Scholz VV, Müller H, Koren K, Nielsen LP, Meckenstock RU (2019) The rhizosphere of aquatic plants is a habitat for cable bacteria. FEMS Microbiol Ecol 95:fiz062

Sulu-Gambari F, Seitaj D, Behrends T, Banerjee D, Meysman FJ, Slomp CP (2016a) Impact of cable bacteria on sedimentary iron and manganese dynamics in a seasonally-hypoxic marine basin. Geochim Cosmochim Acta 192:49–69

Sulu-Gambari F, Seitaj D, Meysman FJ, Schauer R, Polerecky L, Slomp CP (2016b) Cable bacteria control iron–phosphorus dynamics in sediments of a coastal hypoxic basin. Environ Sci Technol 50:1227–1233

Thamdrup B (2000) Bacterial manganese and iron reduction in aquatic sediments. In: Schink B (ed) Advances in microbial ecology, Vol 16. Springer, Boston, MA, p 41–84

van de Velde S, Lesven L, Burdorf LD, Hidalgo-Martinez S and others (2016) The impact of electrogenic sulfur oxidation on the biogeochemistry of coastal sediments: a field study. Geochim Cosmochim Acta 194:211–232

Vasquez-Cardenas D, van de Vossenberg J, Polerecky L, Malkin SY and others (2015) Microbial carbon metabolism associated with electrogenic sulphur oxidation in coastal sediments. ISME J 9:1966–1978

Waugh S, Aller RC (2017) N_2 production and fixation in deep-tier burrows of *Squilla empusa* in muddy sediments of Great Peconic Bay. J Sea Res 129:36–41

Yin H, Zhu Q, Aller RC (2017) An irreversible planar optical sensor for multi-dimensional measurements of sedimentary H_2S. Mar Chem 195:143–152

Yin H, Aller RC, Zhu Q, Aller JY (2021) The dynamics of cable bacteria colonization in surface sediments: a 2D view. Sci Rep 11:7167

Zhu Q, Aller RC, Fan Y (2005) High-performance planar pH fluorosensor for two-dimensional pH measurements in marine sediment and water. Environ Sci Technol 39: 8906–8911

Zhu Q, Aller RC, Fan Y (2006a) Two-dimensional pH distributions and dynamics in bioturbated marine sediments. Geochim Cosmochim Acta 70:4933–4949

Zhu Q, Aller RC, Fan Y (2006b) A new ratiometric, planar fluorosensor for measuring high resolution, two-dimensional pCO_2 distributions in marine sediments. Mar Chem 101:40–53

Editorial responsibility: Erik Kristensen, Odense, Denmark
Reviewed by: S. van de Velde and 2 anonymous referees

Submitted: September 2, 2020
Accepted: April 7, 2021
Proofs received from author(s): June 28, 2021